Journal of Magnetic Resonance **144,** 316–321 (2000)
doi:10.1006/jmre.2000.2060, available online at http://www.idealibrary.com on IDEAL®

# Adiabatic Decoupling Sidebands

Shanmin Zhang and David G. Gorenstein

*Sealy Center for Structural Biology and the Department of Human Biological Chemistry and Genetics, University of Texas Medical Branch, Galveston, Texas 77555-1157*

E-mail: shanmin@tesla.utmb.edu

Received December 6, 1999; revised February 28, 2000

**An analytical solution is given for amplitudes and phases of adiabatic decoupling sidebands as a function of spin inversion time $\tau$. Since all the adiabatic decoupling phases $\vartheta(t, \tau)$ refocus at two periods ($2T$) of the decoupling pulse, the sidebands are located at $n/2T$ rather than at $n/T$ as observed in other decoupling schemes. The real ($R_n(\tau)$) and imaginary ($I_n(\tau)$) amplitudes of the sidebands have symmetry $R_n(\tau) = R_{-n}(\tau)$ and $I_n(\tau) = -I_{-n}(\tau)$, forming a mirror image between the counterparts of the sidebands. When frequency sweep changes direction all $I_n(\tau)$ are inverted while all $R_n(\tau)$ remain unchanged, leading to pure absorption sidebands with two accumulations as demonstrated by Kupče and Freeman, and to an exchange of sidebands between counterparts. The sum of the real parts for sidebands $n = 1$ and 2 is almost a constant near on-resonance decoupling, and it increases substantially for large decoupling offsets. The phase defocusing can be minimized for all decoupling offsets by inserting an initial decoupling period with $T_{ini} = T/2$, eliminating all sidebands located at $n/2T$ ($n = \pm 1, \pm 3, \pm 5, \ldots$).** © 2000 Academic Press

*Key Words:* **adiabatic decoupling sidebands and phases; adiabatic decoupling; subharmonic sidebands; minimizing phase defocusing; suppression of decoupling sidebands.**

## INTRODUCTION

It is well known that adiabatic decoupling (*1–7*) is currently the most efficient decoupling scheme as defined by the ratio of the decoupling range $\Delta f$ divided by the decoupling strength $f_{1rms}$. This is important because it minimizes sample heating, which can be a particular problem at very high field strengths. As a matter of fact, adiabatic decoupling has reached the highest decoupling index ($n = 2$), defined by the relationship $\Delta f = \lambda(f_{1rms})^n$, where $\lambda$ is a constant (*8*). It also has a superb decoupling profile with quite a flat top and very sharp edges, reducing disturbances, including the Bloch–Siegert shift (*9–15*), to the NMR lines outside the decoupling range. It is extremely suitable for homonuclear decoupling at high magnetic fields (*15–18*). In addition, adiabatic decoupling is rather insensitive to the RF field strength and inhomogeneity as long as it satisfies the adiabatic condition (*19*). However, adiabatic decoupling introduces significant sidebands (*15, 18, 20–24*) due mainly to the relatively long adiabatic inversion period compared to the inverse of the sampling rate or dwell time. Unlike other decoupling schemes, adiabatic decoupling inverts the $S$ spins (coupled to the detecting $I$ spins) consecutively when decoupling frequency sweeps from one side of the decoupling offset to the other, resulting in an inversion profile that is unique to a particular type of adiabatic decoupling scheme employed. Consequently, an offset- and sweep-direction-dependent phase accumulation is introduced, which causes an offset- and sweep-direction-dependent variation in amplitudes and phases of all sidebands as demonstrated by Kupče and co-workers (*20–23*). In addition to the multiple sidebands flanked at integer ($n$) multiple frequencies of $n(1/T)$ ($T$ denotes the period of the decoupling pulse) as seen in many other decoupling schemes, half-integer sidebands at $\pm 1/2T$, identified as subharmonic sidebands (*20–23*), are also observed, under off-resonance decoupling conditions.

In homonuclear adiabatic decoupling, however, it was shown that the antisymmetric sidebands are created mainly by the direct irradiation of the nearby decoupling field, which also introduces Bloch–Siegert shifts of all peaks. The nature and amplitudes of the antisymmetric sidebands have been discussed thoroughly (*15, 18*). The relatively small symmetric sidebands, as a result of the modulation of the homonuclear coupling by the decoupling pulse, bear features similar to those that result from the heteronuclear decoupling.

The adiabatic decoupling sidebands were noticed immediately after the adiabatic decoupling was put into use. So far, a number of schemes, including varying decoupling periods (*24*), bilevel decoupling (*21*), ECHO-WURST (*22*), adiabatic defocusing (*23*), phase-cycling algorithms (*25*), etc., were developed to suppress the sidebands. In addition, the coherence sidebands introduced by the antiphase and/or double-quantum coherences created prior to the adiabatic decoupling (*26*) were reduced significantly by gradient dephasing applied just before acquisition (*27*). Using a "BEST" adiabatic decoupling scheme, the cyclic irradiation sidebands mentioned above together with the Bloch–Siegert shift were reduced remarkably by a compensating field and initial decoupling pulses (*15, 18*).



1090-7807/00 $35.00

Even though considerable attention was paid to adiabatic decoupling, there is not a general solution for amplitudes and phases of adiabatic decoupling sidebands, except for on-resonance decoupling (*22*). To achieve such a solution, a unique parameter characterizing all adiabatic decoupling schemes must be identified first; otherwise any solution may be suitable only for a particular decoupling scheme.

In this contribution, an analytical solution for amplitudes and phases of decoupling sidebands as a function of inversion time $\tau$ (a unique parameter for all adiabatic decoupling schemes) is derived for arbitrary adiabatic sweep schemes, such as WURST decoupling with a constant frequency sweep (*4*) and many other sweep schemes (*3, 5, 7*). The unique features of these offset- and sweep-direction-dependent sidebands are explored in detail. We also show how to minimize phase defocusing by inserting initial decoupling pulses, which eliminate all the sidebands located at $n/2T$ with $n = \pm 1, \pm 3, \pm 5, \ldots$.

## CALCULATION OF ADIABATIC DECOUPLING SIDEBANDS

We consider a spin $I$ $(=1/2)$ coupled to a spin $S$ $(=1/2)$ with a coupling constant $J$. Initially, the $I$ spin has a transverse magnetization or single-quantum coherence represented by $I_x$ and it evolves for a time $\tau$ under the interaction of $2\pi JI_zS_z$, which can be described by a density operator formalism (*28, 29*),

$$\sigma(\tau) = e^{-i(2\pi JI_zS_z)\tau} I_x e^{i(2\pi JI_zS_z)\tau}. \qquad [1]$$

At time $\tau$, the $S$ spin is flipped by an adiabatic decoupling pulse. Here we assume that the spin flip occurs instantaneously, which is valid if the duration for spin flip $\delta t$ is much smaller than the period $T$ of the decoupling pulse, i.e., $\delta t/T \ll 1$. To satisfy the adiabatic condition, the sweep range $\delta f = \overline{(df/dt)}\delta t$ [$\overline{(df/dt)}$ stands for average sweep rate] should be comparable to $f_{1\max}$, leading to an expression $\{f_{1\max}/[\overline{(df/dt)}T]\} \ll 1$. For a constant frequency sweep such as used in the WURST decoupling (*4*), $\overline{(df/dt)}T = \Delta f$ (the total frequency sweep) and the condition for instantaneous spin flip reduces to the expression $(f_{1\max}/\Delta f) \ll 1$.

The effect of the instantaneous $S$ spin flip is then equivalent to a 180° pulse applied to the $S$ spin and the density operator can be written as

$$\sigma(\tau) = e^{-i\pi S_x} e^{-i(2\pi JI_zS_z)\tau} I_x e^{i(2\pi JI_zS_z)\tau} e^{i\pi S_x}. \qquad [2]$$

Afterward, $\sigma(\tau)$ evolves continually until the next spin flip occurs at time $\tau + T$. And then, it evolves further to $2T$. The whole process can be described as (*28, 29*)

$$\begin{aligned}\sigma(2T) &= e^{-i(2\pi JI_zS_z)(T-\tau)} e^{-i\pi S_x} e^{-i(2\pi JI_zS_z)T} e^{-i\pi S_x} e^{-i(2\pi JI_zS_z)\tau} I_x \\ &\quad \times e^{i(2\pi JI_zS_z)\tau} e^{i\pi S_x} e^{i(2\pi JI_zS_z)T} e^{i\pi S_x} e^{i(2\pi JI_zS_z)(T-\tau)} \\ &= e^{-i(2\pi JI_zS_z)(T-\tau)} e^{i(2\pi JI_zS_z)T} e^{-i(2\pi JI_zS_z)\tau} I_x \\ &\quad \times e^{i(2\pi JI_zS_z)(T-\tau)} e^{-i(2\pi JI_zS_z)T} e^{i(2\pi JI_zS_z)\tau} = I_x. \end{aligned} \qquad [3]$$

Equation [3] demonstrates that the density operator is refocused after $2T$ no matter when the $S$ spin flips. Therefore, the adiabatic decoupling, in general, has a decoupling period $2T$ rather than $T$.

It follows from Eq. [3] that the density operator within a time $2T$ can be expressed as

$$\sigma(t, \tau) = I_x \cos[\vartheta(t, \tau)] + 2I_yS_z \sin[\vartheta(t, \tau)], \qquad [4]$$

where the adiabatic decoupling phase $\vartheta(t, \tau)$ is defined as

$$\vartheta(t, \tau) = \begin{cases} \alpha t, & 0 \le t \le \tau \\ \alpha(2\tau - t), & \tau \le t \le T + \tau \\ \alpha(t - 2T), & T + \tau \le t \le 2T \end{cases}, \quad 0 \le \tau \le T \quad \text{and} \quad \alpha = \pi J. \qquad [5]$$

In deriving Eq. [4], the following formulas (*30*) are used:

$$\cos(\vartheta S_z) = \cos(\vartheta/2), \qquad [6a]$$

$$\sin(\vartheta S_z) = 2S_z \sin(\vartheta/2). \qquad [6b]$$

The free induction decay (FID) can be calculated directly from Eq. [4],

$$\begin{aligned}\mathrm{FID}(t) &\propto \mathrm{Tr}\{\sigma(t, \tau)(I_x + iI_y)\} \\ &\propto \cos[\vartheta(t, \tau)]. \end{aligned} \qquad [7]$$

Regardless of the inversion time $\tau$, $\vartheta(t, \tau)$ has a period $2T$ and $\vartheta(0, \tau) = \vartheta(2T, \tau) = 0$ as shown in Fig. 1. For $\tau = T/2$, $\cos[\vartheta(t, T/2)]$ has a period of $T$ and $\vartheta(0, T/2) = \vartheta(T, T/2) = 0$, which is referred to as on-resonance decoupling. Also $\vartheta(t, \tau)$ is antisymmetric with respect to $\tau$ in the sense of

$$\vartheta(t, \tau) = -\vartheta(2T - t, T - \tau), \quad 0 \le t \le T. \qquad [8]$$

Except for on-resonance decoupling, the fundamental frequency of the sidebands is $1/2T$ and all the higher order sidebands are thus located at $n/2T$.

The relative amplitudes of all the sidebands as a function of inversion time $\tau$ can be calculated directly from the FID($t$) (Eq. [7]),

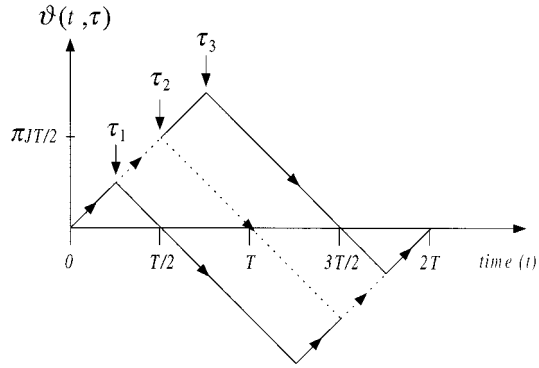


**FIG. 1.** Evolution of the adiabatic decoupling phase $\vartheta(t, \tau)$ (Eq. [5]) for three different inversion times $\tau$. $\tau_1 < T/2$, $\tau_2 = T/2$ (dashed lines), and $\tau_3 > T/2$. For $\tau_2 = T/2$, the phase defocusing has a minimum, i.e., $|\vartheta(t, T/2)|_{\max} = \pi JT/2$. $\vartheta(t, \tau)$ always refocuses at time $2T$ independent of the inversion time $\tau$.

$$R_n(\tau) = \frac{1}{2T}\int_0^{2T} \cos[\vartheta(t, \tau)]\cos(n\pi t/T)dt, \quad \text{Real,} \tag{9a}$$

$$I_n(\tau) = \frac{1}{2T}\int_0^{2T} \cos[\vartheta(t, \tau)]\sin(n\pi t/T)dt, \quad \text{Imaginary.} \tag{9b}$$

With the symmetry of $\vartheta(t, \tau)$ (Eq. [8]), one can show that

$$I_n(T-\tau) = \frac{1}{2T}\int_0^{2T} \cos[\vartheta(t, T-\tau)]\sin(n\pi t/T)dt$$

$$= \frac{1}{2T}\int_0^{2T} \cos[-\vartheta(2T-t, \tau)]\sin(n\pi t/T)dt. \tag{10}$$

By introducing a new variable $u = 2T - t$, one obtains

$$I_n(T-\tau) = -\frac{1}{2T}\int_0^{2T} \cos[\vartheta(u, \tau)]\sin(n\pi u/T)du$$

$$= -I_n(\tau). \tag{11a}$$

Similarly, it is easy to show that

$$R_n(T-\tau) = R_n(\tau). \tag{11b}$$

From Fig. 1 one can see that if the frequency is swept from one side to the other and a spin flip occurs at time $\tau$, the spin flip will occur at time $T - \tau$ if the sweep changes direction. Equations [11a] and [11b] show that the imaginary components of the sidebands $I_n(\tau)$ change sign when sweep changes direction, while the real components $R_n(\tau)$ remain the same. It follows that $I_n(\tau)$ will cancel and $R_n(\tau)$ will add if the two experimental results with different sweep directions are accumulated as shown experimentally by Kupče *et al.* (*21*).

With some tedious calculation, we find analytical solutions for both the real and the imaginary sidebands as a function of inversion time $\tau$,

$$R_n(\tau) = \frac{\alpha T}{(\alpha T)^2 - (n\pi)^2}\{\sin(\alpha\tau)\cos(n\pi\tau/T) + \sin[\alpha(T-\tau)]\cos[n\pi(1+\tau/T)]\} \tag{12a}$$

$$I_n(\tau) = \frac{\alpha T}{(\alpha T)^2 - (n\pi)^2}\{\sin(\alpha\tau)\sin(n\pi\tau/T) + \sin[\alpha(T-\tau)]\sin[n\pi(1+\tau/T)]\} \tag{12b}$$

for $\alpha \neq n\pi/T$, and for $\alpha = n\pi/T$ or $J = n/T$ ($n \neq 0$),

$$R_n(\tau) = \frac{1}{4}[1 + \cos(2n\pi\tau/T)], \tag{13a}$$

$$I_n(\tau) = \frac{1}{4}\sin(2n\pi\tau/T). \tag{13b}$$

The relative phases of the sidebands can be calculated as

$$\varphi_n(\tau) = \tan^{-1}[I_n(\tau)/R_n(\tau)]. \tag{14}$$

Since all the amplitudes and phases are expressed as a function of inversion time $\tau$, the solution is general and is independent of particular types of adiabatic decoupling schemes.

As shown in Eqs. [12a] and [12b], the counterparts of the sidebands have a symmetry of

$$R_n(\tau) = R_{-n}(\tau), \tag{15a}$$

$$I_n(\tau) = -I_{-n}(\tau), \tag{15b}$$

forming a mirror image between the counterparts of the sidebands. The counterparts exchange if the frequency sweep changes direction.

To understand the field ($B_0$) dependence of the adiabatic decoupling sidebands, we consider the case of on-resonance decoupling ($\tau = T/2$) and calculate the nonzero lowest order sidebands. It is straightforward to derive from Eqs. [12a] and [12b] that

$$R_{\pm1}(T/2) = 0, \quad I_{\pm1}(T/2) = 0, \quad I_{\pm2}(T/2) = 0, \tag{16a}$$

and

$$R_{\pm 2}(T/2) = \frac{2JT}{\pi[4 - (JT)^2]} \sin(\pi JT/2). \qquad [16b]$$

For $JT \ll 1$,

$$R_{\pm 2}(T/2) \approx \frac{(JT)^2}{4}. \qquad [17]$$

Equation [17] indicates that one of the effective ways to reduce the intensities of the adiabatic sidebands is to reduce the decoupling period $T$.

When $B_0$ increases, the spread of chemical shift increases linearly and so does the decoupling range. Assuming that the rate of frequency sweep remains the same, the decoupling period $T$ has to increase linearly in order to cover the increased decoupling range. It follows that the sidebands

$$R_{\pm 2}(T/2) \propto B_0^2. \qquad [18]$$

The problem of adiabatic decoupling sidebands is thus much more severe at high magnetic fields.

As pointed out earlier (*18*), the subharmonic sidebands ($n = \pm 1$) can be removed by inserting an initial decoupling with a period $T_{\text{ini}} = T/2$. The initial decoupling period, however, must have the same frequency sweep pattern, range, and direction as the main decoupling, which ensure that if a spin flip occurs at $\tau$ in the main decoupling period, the spin flip will occur at $\tau/2$ in the initial decoupling period. Therefore, the density operator at the time of $\tau + T/2$ can be expressed as

$$\begin{aligned}\sigma(\tau + T/2) &= e^{-i\pi S_x} e^{-i(2\pi JI_zS_z)[\tau+(T-\tau)/2]} e^{-i\pi S_x} e^{-i(2\pi JI_zS_z)(\tau/2)} I_x \\ &\quad \times e^{i(2\pi JI_zS_z)(\tau/2)} e^{i\pi S_x} e^{i(2\pi JI_zS_z)[\tau+(T-\tau)/2]} e^{i\pi S_x} \\ &= e^{i(2\pi JI_zS_z)(T/2)} I_x e^{-i(2\pi JI_zS_z)(T/2)}. \qquad [19]\end{aligned}$$

Equation [19] shows that all the $S$ spins, no matter when they flip, accumulate the same phase $\vartheta(\tau + T/2) = -\pi JT/2$ at their individual flip time $\tau + T/2$, where $\vartheta(\tau + T/2)$ turns out to be the phase minimum. Afterward, the $I$ spins will evolve freely for a period $T$ where they reach a phase maximum $\vartheta(\tau + 3T/2) = \pi JT/2$ and then spin flip as shown in Fig. 2. Similar to the adiabatic defocusing scheme (*23*), the phase defocusing or deviation is therefore minimized, leading to a most effective decoupling. Besides, after a time $T/2 + \tau$ all $\cos[\vartheta(t, \tau)]$, disregarding the inversion time $\tau$, have the same period $T$ instead of $2T$. Consequently, all the sidebands located at $n/2T$ with $n = \pm 1, \pm 3, \pm 5, \ldots$, will disappear.

On the contrary, if the sweep direction of the initial decoupling pulse is opposite to that of the main decoupling, the sidebands will be enhanced instead of eliminated since the phase defocusing is enhanced, except for on-resonance decoupling ($\tau = T/2$), for which it is invariant under changes of sweep directions.

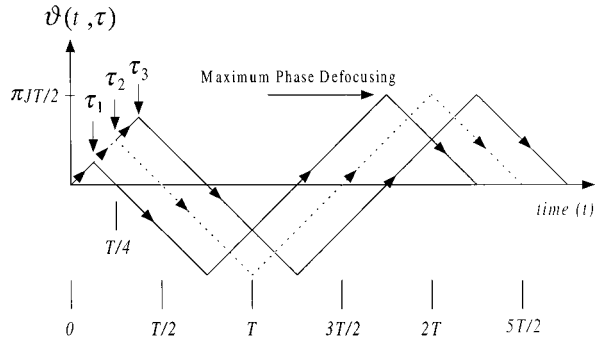


**FIG. 2.** Evolution of the adiabatic decoupling phase $\vartheta(t, \tau)$ for a decoupling scheme of $[T/2]$-Main-Decoupling. Since the initial decoupling period has the same frequency sweep as the main decoupling if a spin flip occurs at a time $\tau$ for the main decoupling, the spin flip will occur at $\tau/2$ for the initial decoupling period. For three different inversion times during the initial decoupling, $\tau_1 < T/4$, $\tau_2 = T/4$ (dashed lines), and $\tau_3 > T/4$, all have the same minimized phase defocusing $|\vartheta(t, \tau)|_{\max} = \pi JT/2$ and the same period $T$ for $\cos(\vartheta(t, \tau))$, after the initial phase evolution.

## EXPERIMENTAL

Experiments were performed on Varian Unity-Plus 750- and 600-MHz NMR instruments with Varian 5-mm HCN triple-resonance probes. A $^{15}$N- and $^{13}$C-labeled (–COOH is unlabeled) *N*-acetylglycine (Fig. 4) in $D_2O$ is used with a single-pulse experiment, detecting the methyl protons and decoupling the directly bonded $^{13}$C. The one-bond heteronuclear coupling constant $^1J(^{13}CH_3) = 139$ Hz. All the decoupling pulses have a WURST-2 decoupling shape $f_1(t) = f_{1\max}[1 - \sin^2(\beta t)]$, $-\pi/2 \le \beta t \le \pi/2$ (*4*). The main adiabatic decoupling has a period $T = 2$ ms, $f_{1\max} = 5.10$ kHz, and $f_{1\text{rms}} = 0.61\, f_{1\max} = 3.11$ kHz. The offset-independent adiabatic decoupling pulse is constructed according to Ref. (*7*) with a 34-kHz frequency sweep, and a phase cycle of (0°, 150°, 60°, 150°, 0°) (*31, 32*).

The real amplitudes $R_n(\tau)$ for $n = 1, 2$ are shown in Fig. 3 together with the experimental results accumulated with two opposite frequency sweep directions. On top, a nonlinear frequency sweep is displayed from −17 to 17 kHz. At $\tau = T/2$, the frequency sweeps passes zero, which corresponds usually to the location of the carrier frequency of the decoupling RF field. As mentioned above, decoupling at this particular position is called on-resonance decoupling. For $n = 1$, the amplitude $R_1(\tau)$ is zero for on-resonance decoupling and it increases symmetrically when the decoupling offset increases or equivalently when $\tau$ deviates from $T/2$. For $n = 2$, the amplitude $R_2(\tau)$ is at maximum for on-resonance decoupling and it decays symmetrically as the decoupling offset increases. At time $\tau = T/4$ and $3T/4$, $R_2(\tau)$ reaches zero and then becomes negative.

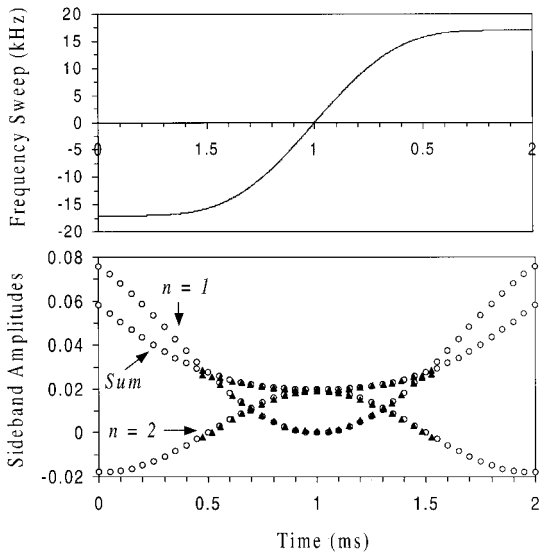


**FIG. 3.** Frequency sweep of the main adiabatic decoupling as a function of decoupling time $t$ (top) and the real sideband amplitudes $R_n(\tau)$ as a function of inversion time $\tau$ (bottom) calculated using Eq. [12a] with $J = 139$ Hz (open circles) and experimental data (solid triangles) for $n = 1$, 2 and the sum of the two. A single-pulse experiment with $^{13}C$ decoupling was employed. The center band of the methyl proton in *N*-acetylglycine is normalized to the calculated value $R_0(T/2) = 0.96852$. The main decoupling has a period $T = 2$ ms and has a WURST-2 decoupling shape $f_1(t) = f_{1max}[1 - \sin^2(\beta t)]$ that is composed of 715 steps.

The sum of the two curves for $n = 1$ and $n = 2$ is shown in Fig. 3. At $\tau = T/2$, the sum has a minimum, which is equal to the maximum of the curve for $n = 2$. Close to the center ($\tau = T/2$), the sum is almost constant as demonstrated experimentally by Kupče and Freeman (*22*). However, it increases symmetrically as $\tau$ deviates from $T/2$ and reaches much higher values at edges contributed by the sidebands for $n = 1$. It will be quite difficult to observe quantitatively the sidebands at edges for $n = \pm 1$ since adiabatic conditions will not be satisfied at edges, and the sidebands will be reduced significantly.

Figure 4 shows the proton spectra (methyl proton region) of *N*-acetylglycine. A 10-kHz decoupling offset is used to exaggerate the subharmonic sidebands (top) obtained with the main adiabatic decoupling. In addition to the subharmonic sidebands located at $\pm 1/2T$, the sidebands located at $\pm 3/2T$ also appear as predicted.

The spectrum in the middle of Fig. 4 is obtained with an initial decoupling period $T_{ini} = T/2$ and the same frequency sweep and direction as the main decoupling. All the sidebands located at $n/2T$, with $n = \pm 1, \pm 3, \pm 5, \ldots$, disappear as discussed above, while the sidebands for $n = \pm 2$ are inverted and the sidebands for $n = \pm 4$ remain unchanged as predicted (*18*).

To cancel sidebands for $n = \pm 2$, two consecutive adiabatic inversions with a period of $T/4$ for each are needed to construct a decoupling scheme $[T/4][T/4][T/2]$-Main-Decoupling. The two consecutive adiabatic inversions $[T/4][T/4]$ cause a complete decoupling cycle (Fig. 1) and refocus all the initial spin states with different decoupling offsets, which ensures that the succeeding decoupling $[T/2]$-Main-Decoupling still has an identical initial spin state and therefore works properly. The sidebands for $n = \pm 2$ will have a 180° phase shift compared with the results obtained by $[T/2]$-Main-Decoupling alone, while the sidebands for $n = \pm 4$ will remain unchanged (*18*). Similarly, to cancel the sidebands for $n = \pm 4$, two additional experiments are required with $[3T/8][3T/8]$ and $[5T/8][5T/8]$ that are added to $[T/2]$-Main-Decoupling, respectively, resulting in two spectra with inverted sidebands for $n = \pm 4$ and

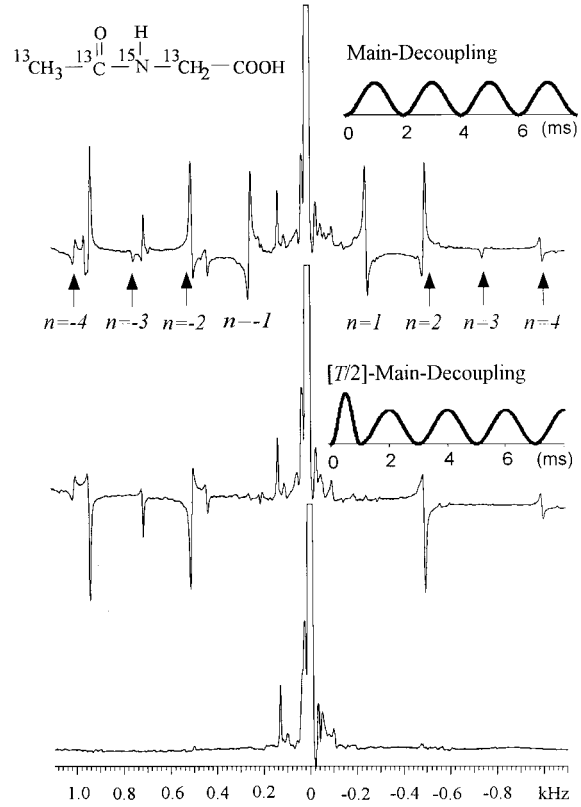


**FIG. 4.** Proton spectra (methyl region) of *N*-acetylglycine using different ($^{13}C$) adiabatic decoupling schemes under a 10-kHz decoupling offset. The spectrum at the top is obtained with the main adiabatic decoupling having a WURST-2 shape, $T = 2$ ms, $f_{1max} = 5.10$ kHz, $f_{1rms} = 0.61\, f_{1max} = 3.11$ kHz, and five phase cycles (0°, 150°, 60°, 150°, 0°). The spectrum shows the decoupling sidebands for $n = \pm 1, \pm 2, \pm 3, \pm 4$ located at $\pm(1/2T)$, $\pm(2/2T)$, $\pm(3/2T)$, and $\pm(4/2T)$, respectively. On the left side, there are some sidebands belonging to the $\alpha$ protons located further downfield. The spectrum in the middle is obtained using an initial decoupling period $T_{ini} = T/2$, i.e., $[T/2]$-Main-Decoupling. All the sidebands located at $n/2T$ for $n = \pm 1, \pm 3, \pm 5, \ldots$, disappear. The sidebands for $n = \pm 2$ are inverted while the sidebands for $n = \pm 4$ remain unchanged. The spectrum at the bottom is obtained with additional initial decoupling periods to invert sidebands for $n = \pm 2$ and $\pm 4$, respectively. A total of four accumulations are used with four different decoupling schemes, i.e., $[T/2]$-Main-Decoupling, $[T/4][T/4][T/2]$-Main-Decoupling, $[3T/8][3T/8][T/2]$-Main-Decoupling, and $[5T/8][5T/8][T/2]$-Main-Decoupling. All the sidebands for $n = \pm 1, \pm 2, \pm 3$, and $\pm 4$ are canceled as predicted.

opposite phase for $n = \pm 2$. Because of reduced intensities and larger offsets, it may not be necessary to cancel the sidebands for $n = \pm 4$. To satisfy the adiabaticity condition (*7*, *20*), the RF strength for different initial decoupling periods $T_{\text{ini}}$ is set according to the formula $f_{1\max}(T_{\text{ini}}) = \sqrt{T/T_{\text{ini}}}\, f_{1\max}$, where $T$ and $f_{1\max}$ are the period and field strength of the main adiabatic decoupling, respectively. For example, the RF strength for an initial decoupling with $T_{\text{ini}} = T/2$ is $f_{1\max}(T/2) = \sqrt{T/(T/2)} f_{1\max} = \sqrt{2} f_{1\max}$. After four accumulations with decoupling sequences of $[T/2]$-Main-Decoupling, $[T/4][T/4][T/2]$-Main-Decoupling, $[3T/8][3T/8][T/2]$-Main-Decoupling, and $[5T/8][5T/8][T/2]$-Main-Decoupling, the sidebands for $n = \pm 2, \pm 4$ and $n = \pm 1, \pm 3, \pm 5, \ldots$ are all eliminated as shown in Fig. 4 (bottom).

## CONCLUSIONS

Adiabatic decoupling sidebands as a function of inversion time $\tau$ can be calculated analytically for arbitrary decoupling schemes. Since the adiabatic decoupling phase $\vartheta(t, \tau)$ refocuses at $2T$, all the sidebands appear at the multiple frequency of $n/2T$ rather than at $n/T$. The sum of the real sidebands for $n = 1$ and $n = 2$ is approximately constant near on-resonance decoupling. However, it increases symmetrically as the decoupling offset increases and reaches much higher values at the edges. Because of the symmetry of the sidebands, $I_n(T - \tau) = -I_n(\tau)$ and $R_n(T - \tau) = R_n(\tau)$, the imaginary parts of the sidebands $I_n$ cancel while the real parts of the sidebands $R_n(\tau)$ add when the spectra from the opposite frequency sweep are accumulated. Also, the counterparts of the sidebands have a symmetry of $R_n(\tau) = R_{-n}(\tau)$ and $I_n(\tau) = -I_{-n}(\tau)$, forming a mirror image of each other about the center and exchanging position between the counterparts when the sweep direction is reversed. The problem of the adiabatic decoupling sidebands becomes more severe at high magnetic fields since $R_{\pm 2}(T/2) \propto B_0^2$. The phase defocusing $|\vartheta(t, \tau)|_{\max}$ can be minimized by inserting an initial decoupling with $T_{\text{ini}} = T/2$ and with the same sweep width and direction as the main decoupling, causing all $\cos[\vartheta(t, \tau)]$ [$\propto \text{FID}(t)$], disregarding the inversion time $\tau$, to have the same period $T$ after an initial phase evolution. Consequently, all the sidebands located at $n/2T$ with $n = \pm 1, \pm 3, \pm 5, \ldots$, disappear. The sidebands for $n = \pm 2, \pm 4$ can also be canceled in four scans with proper additional initial decoupling periods. The scheme of inserting initial decoupling pulses can also be applied to double-band adiabatic decoupling, such as in Double-WURST decoupling (*8*), with frequency-shifted (*33*) decoupling in one decoupling band.

## ACKNOWLEDGMENTS

This research was supported by NIH (AI27744), NIEHS (ES06676), the Welch Foundation (H-1296), the Lucille P. Markey Foundation, and the Sealy and Smith Foundation. Building funds were provided by NIH (1CO6CA59098).

## REFERENCES

1. M. S. Silver, R. I. Joseph, C.-N. Chen, V. J. Sank, and D. I. Hoult, *Nature* **310,** 681 (1984).
2. J. Baum, R. Tyko, and A. Pines, *Phys. Rev. A* **32,** 3435 (1985).
3. M. R. Bendall, *J. Magn. Reson. A* **112,** 126 (1995).
4. Ē. Kupče and R. Freeman, *J. Magn. Reson. A* **115,** 273 (1995).
5. R. Fu and G. Bodenhausen, *J. Magn. Reson. A* **117,** 324 (1995).
6. Ē. Kupče and G. Wagner, *J. Magn. Reson. B* **110,** 309 (1996).
7. A. Tannús and M. Garwood, *J. Magn. Reson. A* **120,** 133 (1996).
8. S. Zhang, J. Wu, and D. G. Gorenstein, *J. Magn. Reson. A* **123,** 181 (1996).
9. F. Bloch and A. Siegert, *Phys. Rev.* **57,** 552 (1940).
10. W. S. Warren, *J. Chem. Phys.* **81,** 5437 (1984).
11. L. Emsley and G. Bodenhausen, *Chem. Phys. Lett.* **168,** 297 (1990).
12. S. Grzesiek and A. Bax, *J. Magn. Reson.* **96,** 432 (1992).
13. M. A. McCoy and L. Mueller, *J. Magn. Reson.* **98,** 674 (1992).
14. G. W. Vuister and A. Bax, *J. Magn. Reson.* **98,** 428 (1992).
15. S. Zhang and D. G. Gorenstein, *J. Magn. Reson.* **132,** 81 (1998).
16. Ē. Kupče and G. Wagner, *J. Magn. Reson. B* **109,** 329 (1995).
17. H. Matsuo, Ē. Kupče, H. Li, and G. Wagner, *J. Magn. Reson. B* **113,** 91 (1995).
18. S. Zhang and D. G. Gorenstein, *J. Magn. Reson.* **138,** 281 (1999).
19. A. Abragam, "Principles of Nuclear Magnetism," Oxford Univ. Press, Oxford (1961).
20. Ē. Kupče and R. Freeman, *J. Magn. Reson. A* **117,** 246 (1995).
21. Ē. Kupče, R. Freeman, G. Wider, and K. Wuthrich, *J. Magn. Reson. A* **122,** 81 (1996).
22. Ē. Kupče and R. Freeman, *J. Magn. Reson.* **127,** 36 (1997).
23. Ē. Kupče, *J. Magn. Reson.* **129,** 219 (1997).
24. T. Hwang, M. Garwood, A. Tannus, and P. C. M. van Zijl, *J. Magn. Reson. A* **121,** 221 (1996).
25. T. E. Skinner and M. R. Bendall, *J. Magn. Reson.* **124,** 474 (1997).
26. M. H. Levitt, G. Bodenhausen, and R. R. Ernst, *J. Magn. Reson.* **53,** 443 (1983).
27. M. R. Bendall and T. E. Skinner, *J. Magn. Reson.* **129,** 30 (1997).
28. R. R. Ernst, G. Bodenhausen, and A. Wokaun, "Principles of Nuclear Magnetic Resonance in One and Two Dimensions," Clarendon Press, Oxford (1987).
29. M. Mehring, "High Resolution NMR Spectroscopy in Solids," Springer-Verlag, Berlin (1976).
30. M. Goldman, "Quantum Description of High-Resolution NMR in Liquids," Clarendon Press, Oxford (1988).
31. R. Tycko, A. Pines, and R. Gluckenheimer, *J. Chem. Phys.* **83,** 2775 (1985).
32. T. Fujiwara and K. Nagayama, *J. Magn. Reson.* **77,** 53 (1988).
33. S. Zhang and D. G. Gorenstein, *J. Chem. Phys.* **105,** 5659 (1996).